Penetration Depth and Flux Creep in Thin Superconducting Indium Films*†

Robert A. Anderson‡ and D. M. Ginsberg
Department of Physics and Materials Research Laboratory, University of Illinois, Urbana, Illinois 61801
(Received 4 November 1971)

We have measured the absolute value of the penetration depth in superconducting indium films. Applying a dc axial magnetic field to the exterior of a hollow superconducting thin-film cylinder, we determined the ratio $\Delta H_i/\Delta H_0$ of the variation of the magnetic field penetrating into the interior region to the variation of the applied magnetic field. Applied magnetic fields of small amplitude were used so that ΔH_i was linear in ΔH_0; a superconducting magnetometer was used to measure ΔH_i. Film thicknesses were between 95 and 160 Å, and the temperature range was from 1.3 K to the critical temperature near 4.0 K. From the actual penetration depths deduced from these measurements, which were performed on four samples, values of the London penetration depth at absolute zero $\lambda_L(0)$ were calculated to be in the range 397 ± 22 Å. This indicates that $\lambda_L(0)$ in thin films is larger than typical published measurements for bulk indium, in accordance with other evidence. Except for one sample and for temperature within about 0.3 K of the critical temperature, the data were fitted moderately well by the theoretical temperature dependence. Flux creep depending logarithmically on elapsed time was also observed for values of ΔH_0 sufficiently large to induce currents in the film exceeding the critical-state current. The temperature dependence of the logarithmic flux-creep rate was approximately that of the product of the critical current, the absolute temperature, and the square of the penetration depth over a wide range of temperatures.

I. INTRODUCTION

We have made absolute measurements of the superconducting penetration depth λ in indium films on the order of 100 Å thick. Both the absolute value of λ and its temperature dependence are of continued interest, and are not yet completely understood.[1,2]

Our experiment was motivated in part by the development of an easily constructed type of quantum-interference device, the Clarke superconducting low-inductance galvanometer (SLUG).[3,4] We designed a superconducting magnetometer circuit incorporating this device, that had a magnetic field sensitivity on the order of 10 μG and a frequency response which effectively extended to zero frequency. Also, the magnetometer was capable of measuring a magnetic field without causing an appreciable field distortion.

The magnetometer was suited to measuring the superconducting penetration depth by determining the attenuation of an applied magnetic field by a thin superconducting film in the form of a hollow cylinder. A variation in a uniform axially aligned external magnetic field H_0 produced a corresponding highly attenuated variation in the magnetic field H_i inside of the cylinder. The magnetometer probe was placed inside the cylinder, and was used to measure the variation of H_i.

One of the main differences between this experiment and similar ones which have been performed on hollow cylinders[5-9] was our use of the superconducting magnetometer and very-low-frequency (0.1 Hz) magnetic field sweeps, rather than pickup coils and ac magnetic fields. An advantage of using very low frequencies is that magnetic field distortions caused by currents induced in the metal parts of the cryostat (including resonant circuits if any) are eliminated.

Operation of the magnetometer at very low frequency also facilitated determinations of the maximum amplitude of the sweep of H_0 for which H_i responded linearly, and allowed straightforward observations of hysteresis effects associated with applied magnetic field sweeps of larger amplitude. While making the first measurements on our samples, we observed a number of phenomena related to the leakage of quantized magnetic field lines through the cylinder wall for large amplitude sweeps of H_0. These phenomena were caused by flux creep which occurred as currents in the sample relaxed toward the critical state[10] following a perturbation of H_0. A fluxoid passing through the film presumably crept toward or away from the ends of the sample. The temperature dependence of the logarithmic flux-creep rate[11,12] $dH_i/d\log_{10}t$ (where t is time) will be reported below.

Another innovation in this experiment was to compensate for field-fringing effects by placing solenoids at the ends of the cylindrical film to extend the sheet of current beyond the ends, approximately simulating an infinitely long cylindrical film. By altering the current flowing in these end solenoids, the effects of field fringing were measured directly. In some of the previous experiments on cylindrical films, the techniques required there to be regions

of the sample with a sizable component of the magnetic field normal to the film's surface.[6,7] This component would force some regions of the film into the mixed state.[13] The effect of this would be impossible to calculate, so it is best avoided when trying to measure λ.

In contrast to the direct measurement of λ reported here, microwave determinations[14] require an analysis which is very complex, and therefore more subject to possible error. Our measurements have been made on thin-film samples, in which the electron mean free path l is much shorter than λ. In this so-called dirty limit, the electromagnetic response is a local one, so experimental results can be compared rather directly with theory in contrast to the treatment required for data obtained for bulk samples.[15] (Penetration-depth measurements can also be made on a film which forms part of a Josephson junction.[16])

Indium was chosen for our investigation partly because lead and tin had been used in other, similar experiments on cylindrical films, and partly because indium films of high quality can be made readily.

II. DETERMINATION OF LONDON PENETRATION DEPTH

In the London model, which is a local model, the current density $\vec{J}$ is proportional to the magnetic vector potential $\vec{A}$. As a consequence, the magnetic field obeys the equation

$$(\nabla^2 - 1/\lambda^2)\vec{H} = 0, \tag{1}$$

where λ is the penetration depth.[1] In the London theory, λ has the value

$$\lambda_L \equiv (mc^2/4\pi n_s e^2)^{1/2}, \tag{2}$$

where m, n_s, and e are the effective mass, number density, and charge of the superconducting electrons, respectively. The solution of Eq. (1) for the geometry of this experiment, taking into account the inductance of the hollow cylinder, is given by

$$\frac{\Delta H_i}{\Delta H_0} = \frac{2\lambda^2/ad}{1 + 2\lambda^2/ad} \tag{3}$$

plus terms which are of order $(d/\lambda)^2$ smaller, where a and d are the film radius and thickness, respectively.

Our films had a radius $a \sim 0.8$ cm and a thickness $d \sim 100$ Å, and were found to attenuate the applied magnetic field signal more than a 1000-fold at low temperatures, so that $\lambda(0)$ was on the order of 1000 Å; this value is several times larger than would be expected for $\lambda_L(0)$ on the basis of the London theory. It is clear that nonlocal effects must be taken into account in interpreting our data. The London penetration depth is a fundamental parameter in nonlocal theories as well as in the (local) London theory; λ_L is still defined by Eq. (2) in the nonlocal theories.

A prediction of the BCS theory,[17,18] is that $\vec{J}$ and $\vec{A}$ are related in a nonlocal way by the equation

$$\vec{J}(\vec{r}) = \frac{-3ne^2}{4\pi mc\,\xi_0} \int \frac{[\vec{A}(\vec{r}\,')\cdot\vec{R}]\vec{R}K(R, T)e^{-R/l}}{R^4}\, d\vec{r}', \tag{4}$$

where $\vec{R} = \vec{r}' - \vec{r}$, n is the number density of conduction electrons, ξ_0 is the ideal coherence length of electron pairs for infinite mean free path, and l is the electron mean free path. The kernel $K(R, T)$ has a spatial dependence similar to that of the function e^{-R/ξ_0}.

Because d and l for our films are considerably smaller than ξ_0, the integral is very insensitive to the difference between the spatial dependence of $K(R, T)$ and that of $e^{-R/l}$. Therefore, Eq. (4) has a spatial dependence which is equivalent to the relation proposed by Pippard.[19] The temperature dependence that applies to our measurements may be found by evaluating $K(R, T)$ at $R = 0$. One obtains[17]

$$K(0, T) = [\Delta(T)/\Delta(0)]\tanh[\Delta(T)/2k_BT], \tag{5}$$

where Δ is the energy gap and k_B is the Boltzmann constant. Mühlschlegel has tabulated BCS values of $\Delta(T)$.[20]

Peter has obtained a nearly exact solution of the Pippard relation for the magnetic field attenuation ratio of a thin-film cylinder, assuming diffusely reflecting film walls and a film thickness less than the penetration depth.[21] This solution may be written in a form similar to that of Eq. (3), namely,

$$\Delta H_i/\Delta H_0 = A(T)/[1 + A(T)], \tag{6}$$

where

$$A(T) = 8\lambda_L^2(0)\,K(0, T)^{-1}\,\xi_0\gamma/3ad^2, \tag{7}$$

$$\gamma^{-1} = 0.423 + (\tfrac{2}{3})\,d/\xi - 0.168(d/\xi)^2 + [1 - (\tfrac{1}{12})(d/\xi)^2]\ln(\xi/d), \tag{8}$$

and

$$\xi = (\xi_0^{-1} + l^{-1})^{-1}. \tag{9}$$

The London penetration depth has been determined from our data with the aid of Eqs. (6)–(9). We assume that $K(0,T)$ can be calculated correctly from Eq. (5) if experimental values of $\Delta(T)$ and $\Delta(0)$ are used, even though indium is not in the weak-coupling limit.

III. EXPERIMENTAL PROCEDURE

A. Sample Production

Each of our samples was deposited under high vacuum onto a cylindrical Pyrex substrate by evaporating 99.999%-pure indium from a hot molybdenum boat in about 10 sec. The substrates were

similar in design to those of Erlbach *et al.*[6,7] The section of tubing onto which the indium was deposited was cooled directly by liquid nitrogen. During the indium film deposition, the substrate was rotated at 20 revolutions/sec. Indium vapor from the hot source passed through a rectangular aperture which was narrower than the substrate diameter; this prevented low-angle deposition. The resulting indium film was a hollow 1.52-cm-diam 3.81-cm-long cylinder. Because the distance from source to substrate was about 23 cm and the indium deposition was made during many rotations of the substrate, the film thickness throughout each sample was uniform to about 1%. The vacuum seal to the rotating substrate was made by a pair of Viton O rings,[22] lubricated with Apiezon *N* grease.[23] The space between the O rings was pumped to remove any air that leaked past the outer one. A pressure not exceeding 2×10^{-6} Torr was maintained in the evaporator during the indium deposition.

A quartz-crystal thickness monitor[24] beside the substrate allowed a rough determination of the film thickness during the deposition, so the desired film thickness could be obtained. Also exposed to the beam of indium atoms was a small glass slide, cooled by being in thermal contact with a liquid-nitrogen cold trap. The thickness of the indium deposit on the glass slide was determined optically by multiple-beam interferometry using Fizeau fringes.[25,26] The film thickness on the cylindrical substrate could be determined by dividing the thickness of the film on the slide by a geometrical factor. A third method of measuring the film thickness, involving the temperature dependence of the electrical resistance, was the method actually used for the final data analysis. We preferred this method to the optical method, because some of the indium film no doubt oxidized while the substrate was being transferred from the evaporator to the cryostat, and this would decrease the actual thickness of the indium metal.

Prior to the deposition of each indium film, the substrate was carefully cleaned. After being scrubbed with detergent and hot water, the substrate was rinsed in rapid succession with deionized water, reagent grade acetone and isopropyl alcohol. Following this, the substrate was placed in a specially designed vapor degreaser, where hot isopropyl alcohol was continuously distilled onto the substrate surface. Final cleaning was accomplished by about 15 min of glow discharge after the substrate had been mounted in the evaporator. A hollow cathode[27] was used, and a stable discharge occurred in air at a pressure of 0.05 Torr at 900 V dc and 40 mA. Apparently the cleaning procedure was effective, as the cylindrical indium films usually appeared uniform in opacity. Visibly imperfect indium films were rejected.

Figure 1 shows a sample which is ready to be mounted in the cryostat. The sample was prepared by cracking off the part of the substrate bearing the indium film, then placing this section twice more into the evaporator to receive silver current- and voltage-contact deposits to be used in the potentiometric measurements of the electrical resistance. The voltage contacts were in line with each other, and were diametrically opposite to the current contacts as shown. Electrical connection to the indium film occurred at a 1-mm-diam semicircular overlap at the tip of each contact. Silver micropaint[28] was used to attach No. 36 copper wires to the other ends of the silver contacts when the sample was mounted in the cryostat. The silver contacts were long enough to protrude about 6 mm from under the 2.54-cm-long end solenoids after they had been slid into place on the sample substrate. To find the resistivity of each film, the resistance per square[29] R was calculated[30] to be given by the expression $R = 2.74V/I$, where V is the voltage across the voltage contacts and I is the current passing through the current contacts.

B. Superconducting Magnetometer

The construction and performance of the Clarke SLUG used in the superconducting magnetometer were similar to those of devices made by Clarke.[3] The magnetometer is shown schematically in Fig. 2. The niobium wire of the SLUG was part of a superconducting closed loop; superconducting niobium zirconium wire[31] formed the rest of the loop. The ends of this wire were stripped to the core material and tightly clamped against the niobium wire to form superconducting connections.

An ac current (10 μA rms at 1000 Hz) was in-

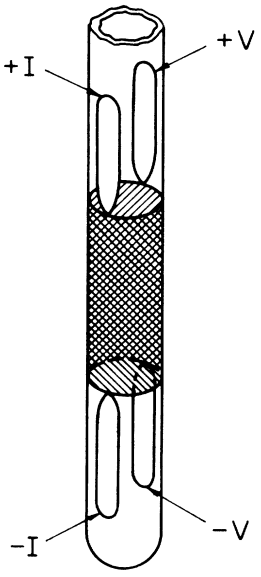

FIG. 1. Sample ready to be mounted in the cryostat. The cylindrical indium film and the silver electrical-contact overlays are shown.

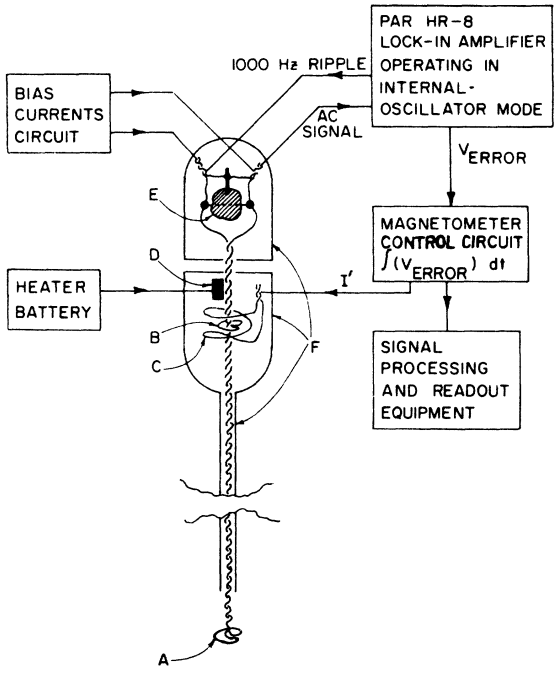

FIG. 2. Schematic drawing of the superconducting magnetometer. A is the probe loop, B is the compensation loop, C is the compensation solenoid, D is the heater, E is the Clarke SLUG, and F is the superconducting magnetic shielding.

jected into the SLUG tunneling-current bias, and the resulting output of the lock-in amplifier was proportional to the dynamic tunneling resistance. The dc component of the tunneling-current bias was adjusted to place the device's operating point on the steep side of the first dynamic-resistance peak.

The principle of operation was as follows. A change in the magnetic field H_i at the probe loop induced a persistent current which passed through the SLUG and altered its dynamic resistance. The consequent change in the output of the lock-in was time integrated and then converted to a current I' that flowed through the compensation solenoid, producing a magnetic field at the compensation loop. The persistent current passing through the probe loop was thereby returned to zero. (Thus, the distortion in the field inside the sample caused by the persistent current in the probe loop was also returned to zero!) After the magnetometer was calibrated (at a temperature above the transition temperature T_c of the sample being run), the change in H_i could be determined from a measurement of the current I'. The magnetometer circuit responded with a time constant of about 0.1 sec, and had a noise level corresponding to a field of about 50 μG rms. A heater allowed part of the superconducting loop to be warmed above its transition temperature so that persistent currents could be caused to decay to zero. The magnetometer could be moved vertically to determine the field homogeneity.

The pair of magnetically shielded chambers shown in Fig. 2 had a roughly elliptical outline to reduce the penetration of the magnetic field into the region of the SLUG and the compensation loop. A thick layer of lead-tin solder coating the chambers provided the shielding. The twisted part of the superconducting wire leading to the probe tip was shielded by a length of single-core lead-tin solder, from which the rosin had been removed to make room for the wire. This shielding was terminated about 4.5 cm from the probe loop so persistent currents in the shielding would not distort the magnetic field inside the sample. Unfortunately, the unshielded part of the twisted wires introduced a stray magnetic field sensitivity which was comparable to the magnetic field penetrating through the sample at low temperatures (on the order of 1 part in 10^3). It was therefore necessary to measure the stray sensitivity for each run by replacing the thin film by a thick cylindrical indium foil, holding everything else fixed. We then corrected the data for the effect of the stray sensitivity.

C. Cryostat Design and Magnetic Field Coils

It was found that the SLUG operated best near 4.2 K; therefore, the cryostat was designed to allow the entire magnetometer to remain in a 4.2-K helium bath while the temperature of the sample film was varied. Part of the cryostat is shown schematically in Fig. 3. (Radiation traps were used, but are not shown.) The two closed-end tubes extending downward from the tops of the inner and outer chambers were thermally isolated by an extension of the vacuum space between the two chambers. These tubes were made of brass; the smaller one held the magnetometer probe, and the sample fitted over the larger one.

Refrigeration for the sample chamber was provided by a copper wire which furnished a thermal link to a liquid-helium reservoir. The reservoir pressure was regulated by a Mylar diaphragm manostat, and was maintained at a temperature about 50 mK below the desired sample-chamber temperature. The temperature of the top of the sample chamber was electronically regulated.[32] Temperatures from 1.3 to 5.0 K, stable to a small fraction of an mK were obtainable. Helium gas at a pressure of about 8 Torr in the sample chamber provided thermal contact. The temperature was measured by a germanium thermometer that had been calibrated according to the T_{58} scale of helium vapor pressure. Electrical leads in the

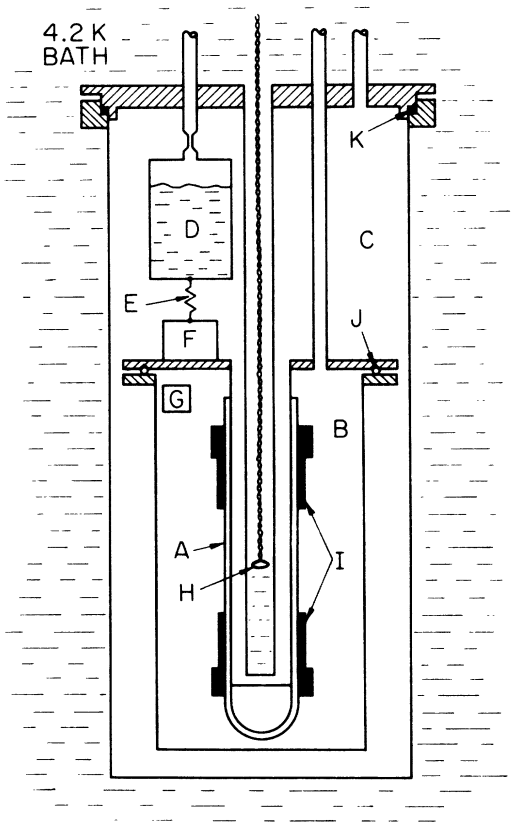

FIG. 3. Schematic drawing of part of the cryostat. A is the sample, B is the sample chamber, C is the vacuum space, D is the liquid-helium reservoir, E is the thermal link, F is the heater and carbon-resistor thermometer, G is the germanium thermometer, H is the magnetometer probe loop, I are the end solenoids, J is the gold O ring, and K is the indium O ring.

sample chamber were thermally anchored to the top of the sample chamber and then passed into the 4.2-K helium bath through an epoxy feedthrough.[33]

Both the sample chamber and the surrounding vacuum chamber were sealed with metal O rings. Because the vacuum chamber was always at 4.2 K, above the superconducting transition temperature of indium, a simple indium-wire seal was used without distorting the magnetic field. A gold wire, covered with a very thin layer of N grease[23] and seated in a V-shaped groove, provided a reliable and reusable seal for the sample chamber.

Magnetic fields were generated by currents in three coil systems, two of which fit around the outside of the nitrogen Dewar. A pair of saddle-shaped coils[34,35] were used to cancel the horizontal component of the ambient magnetic field. It was not necessary to cancel the vertical component of the ambient field, as it was aligned with the sample axis. An array of four coils, which will be called the main-field coils, were specially designed to provide a vertical magnetic field H_0 of high uniformity in the volume occupied by the sample. These were aligned in the axial direction to within 0.1° by monitoring the sample's resistive transition. The third coil system was comprised of the end solenoids, the purpose of which was described in Sec. I. They were No. 34 insulated copper wire, wound one layer deep along most of their length. As shown schematically in Fig. 3, they had extra windings at their outer ends, which compensated for their finite length.

D. Acquisition of Magnetic Data

During the measurement of the magnetic field attenuation ratios, the main-field coils and end solenoids were driven by a function generator. The applied magnetic field signal was a symmetrical triangle wave with a period of about 10 sec. Using an on-line signal averager,[36] we averaged from 8 to 64 complete waveforms (depending on the amount of noise rejection needed) of the voltage signal from the magnetometer control circuit, which was proportional to I', and therefore to H_i. After the signals had been accumulated, the symmetry of the waveform was used to advantage: The contents of the second half of the signal averager were automatically subtracted channel by channel from the contents of the first half. In this way the effective number of averaged signals was doubled and long-period drift in the voltage signal from the magnetometer was canceled to first order. The first half of the memory was then read onto an X-Y recorder, producing a curve that was an inclined straight line (plus noise). Whenever the amplitude of the H_0 sweep had been too large, the resulting hysteresis was evident as curvature in the plot. It was found that the maximum usuable amplitude of the H_0 sweep depended on temperature roughly as $T_c - T$, and was about 50 to 500 mG for samples 1 and 4, respectively, at 2.0 K. Best-fitting straight lines, estimated by eye, were determined later for each of the recorded curves, and the magnetic field attenuation ratios were obtained from the slopes of these lines.

To measure hysteresis effects for large amplitude field sweeps, the signal from the magnetometer was fed directly to the Y axis of the recorder. (During these measurements the current to the end solenoids was turned off.) Hysteresis loops, from which the temperature dependence of the critical current was estimated, were drawn by feeding into the X channel of the recorder a voltage proportional to H_0. However, for the time-dependent-flux-creep measurements, the X axis was swept at a constant rate of 2.54 mm/sec. The function generator was used to drive the main-field coils

at temperatures near T_c, where the generator's output was sufficiently large to produce field-sweep amplitudes which could induce currents in the thin-film sample exceeding the critical-state currents. At lower temperatures, the main-field coils were driven by a manually controlled dc power supply.

Both the acquisition and the reduction of the flux-creep data were somewhat complex. To take reproducible data, the applied magnetic field had to be swept far enough to drive the film past the critical state. Then the sweep had to be stopped abruptly, without reversal of direction, and with the recorder pen on scale in the Y direction. It was necessary to turn off the magnetometer and to energize the superconducting-loop heater during the large changes in H_0 needed to exceed the critical-state current at lower temperatures. To analyze the data, the curves were first digitized[37]; then a computer program was used to interpolate the curves and replot them with a logarithmic-time axis. The logarithmic-creep rates were obtained from the slopes of the computer-plotted curves.

E. Film-Thickness Determination

To determine the film thickness from measurements of resistance vs temperature, we used Fuchs's expression for the resistivity of a thin film,[38] which may be written

$$\rho(d, T)/\rho(\infty, T) = F(x) , \tag{10}$$

where

$$\frac{1}{F(x)} = 1 - \frac{3}{8x} + \left(\frac{3}{8x} - \frac{5}{8} + \frac{x^2 - x}{16}\right) e^{-x} + \frac{3x}{4}\left(1 - \frac{x^2}{12}\right) \int_x^\infty t^{-1} e^{-t}\, dt . \tag{11}$$

The functions $\rho(d, T)$ and $\rho(\infty, T)$ are the resistivities at temperature T of a film of thickness d and of bulk material with the same composition as the film, respectively; x is defined to be $d/l(\infty, T)$, where $l(\infty, T)$ is the electron mean free path in bulk material with the same composition as the film. The derivation of Eqs. (10) and (11) assumes diffuse scattering of the electrons from plane-parallel film surfaces and isotropic scattering inside the film.

For low concentrations of impurities the product ρl is expected to be approximately independent of temperature and impurity content. Also, the total resistivity of a bulk material at a temperature T may be approximated by the sum of the residual resistivity due to impurity scattering $\rho(\infty, 0)$, and the resistivity of a pure bulk sample of the material $\rho_{pb}(T)$, according to Matthiessen's rule. From these relations, it is easy to show that the resistance per square of the film $R = \rho/d$ is given by

$$R(T) = xF(x)\rho l/d^2 , \tag{12}$$

where

$$x = d[1/l(\infty, 0) + \rho_{pb}(T)/\rho l] . \tag{13}$$

An electronic calculating machine was programmed to solve Eqs. (12) and (13) for d and $l(\infty, 0)$, given the quantity ρl and the values of $R(T)$ and $\rho_{pb}(T)$ for two different temperatures. We used the resistance at room temperature and the residual resistance of the indium film for the two values of $R(T)$. The value of $\rho_{pb}(T)$ at room temperature was obtained by interpolating the data of White and Woods,[39] taking ρ_{pb} (273.2 K) to be 8.1 $\mu\Omega$ cm.[39–41] The value of $\rho_{pb}(T)$ near 5 K was set equal to zero. (Nonisotropic phonon scattering below the Debye temperature[42] did not need to be taken into account because phonon scattering did not contribute to ρ significantly near 5 K.)

Published values of ρl for indium vary by a factor of about 3.[43–55] Therefore, d and l were determined for ρl values of 700, 1100, and 1500 $\mu\Omega$ cm Å. We have chosen to focus attention on the value 1100 $\mu\Omega$ cm Å, which is in agreement with recent anomalous-skin-effect measurements on polycrystalline samples,[44] thin-film-resistance size-effect measurements,[45,48] and thin-film critical-field measurements.[49] However, if these results are averaged with larger values of ρl from an assortment of experiments involving size effects in small specimens,[46,50–54] a value of 1300 $\mu\Omega$ cm Å might seem better. We measured the film resistance at several temperatures between 5 K and room temperature. These data were found[30] to be fitted rather well by Eq. (12) for values of ρl between 1300 and 1700 $\mu\Omega$ cm Å, although the nonisotropic phonon scattering may have slightly affected the results.

IV. RESULTS

A. Film Thicknesses, Mean Free Paths, and Resistive Transitions

Values for the film thickness and low-temperature electron mean free path are listed in Table I. They were determined as described in Secs. III A and III E. In the Table, the mean free path listed is $l(\infty, 0)$, that expected for a bulk sample with the same composition as the film in the residual-resistance range of temperatures.

It is clear that the optically determined values for the film thickness are consistently on the order of 20 Å greater than the $R(T)$ thicknesses. We presume that this difference in thickness resulted from the formation of an oxide layer during the time in which the sample was exposed to air at room temperature, although surface roughness may have been a contributing factor. We have therefore chosen to rely on the values of film thickness which were determined from $R(T)$.

The transition temperature T_c and transition width

TABLE I. Film thicknesses, mean free paths, and resistive transitions.

Sample	Optically determined thickness (Å)	Thickness from $R(T)$ $\rho l(\mu\Omega$ cm Å) = 700	1100	1500	Mean free path from $R(T)$ $\rho l(\mu\Omega$ cm Å) = 700	1100	1500	T_c (K)	δT_c (mK)
1	119.6	90.3	95.2	101.0	199.9	437.3	758.0	3.958	55
2	135.1	94.5	100.4	106.9	270.5	613.2	1089.9	3.884	122
3	146.7	133.3	136.3	141.6	174.4	369.3	637.9	3.994	28
4	171.3	157.4	160.2	165.7	198.6	422.6	738.0	3.942	37

δT_c are also listed in Table I. T_c for a given sample is defined as the temperature at which the sample's electrical resistance was one-half of the residual resistance. We define δT_c as the width of the temperature interval in which the sample's resistance rose from 10% to 90% of the residual resistance. It is thought that the sizable magnitude of δT_c is an indication of sample inhomogeneities, possibly introduced by strains which were created by differential contraction as the samples were cooled from room temperature.

B. London Penetration Depth at Absolute Zero

The London penetration depth at absolute zero $\lambda_L(0)$ for each of our samples was determined by an extrapolation to absolute zero of a least-squares fit of Eq. (6) to the measured magnetic field attenuation ratio in the range from 1.3 (the lowest attainable temperature) to 1.8 K. The choice of 1.8 K as the highest temperature of data included in the least-squares fit was a compromise between including enough data to provide good statistics and avoiding the temperature range where the theoretical temperature dependence was appreciably affected by the detailed model (see below). The reduced energy gap $2\Delta(0)k_BT_c$ was taken to be 3.69 for indium from recent tunneling measurements.[56] Our results are listed in Table II.

In using Eq. (6) to find $\lambda_L(0)$, one must know ξ_0, the ideal coherence length. Published values for ξ_0 vary widely, from 2000 to 4400 Å.[43,45,48,49,55,57] Taking the free-electron value for the Fermi velocity, the coherence length according to BCS theory is about 7000 Å. However, if the Fermi velocity is renormalized[58] according to observed values of the specific-heat coefficient and the free area of the Fermi surface, ξ_0 becomes 2460 Å. Although we believe that 2500 Å is a reasonable value for ξ_0, Table II lists values of $\lambda_L(0)$ calculated for a range of values of ξ_0. Because ξ_0 varies inversely with T_c according to the theory, the value of ξ_0 used in Eq. (6) was the bulk value multiplied by the ratio of the bulk transition temperature to that of the sample film. The transition temperature of the film was taken to be the temperature for which the electrical resistance was 50% of the residual resistance (that just above the transition temperature). Because $\lambda_L(0)$ also depends implicitly on ρl through the dependence on d and l in Eq. (6), and because ρl is not precisely known (see Sec. III

TABLE II. Penetration depths.

Sample	$10^4A(0)$	$\lambda(0)$ (Å) meas.	$\lambda(0)$ (Å) calc.	ρl ($\mu\Omega$ cm Å)	$\lambda_L(0)$ (Å) for ξ_0(Å) = 2000	2500	3000	3500	4000	$\lambda_L(0)$ (Å) from temp. dependence[a]
1	6.81	1570	1477	700	357	321	294	273	256	
				1100	439	396	364	338	318	396
				1500	502	455	419	390	367	
2	5.31	1423	1371	700	347	312	286	266	249	
				1100	424	383	353	328	308	396
				1500	482	438	404	377	355	
3	3.76	1396	1387	700	339	305	279	259	243	
				1100	415	375	344	320	301	361
				1500	475	430	396	369	347	
4	3.54	1468	1297	700	380	342	313	291	273	
				1100	464	419	386	359	337	353
				1500	529	480	443	413	389	

[a]Calculated to best fit the temperature dependence of $\lambda(T)$ at low temperature, assuming $2\Delta(0)/kT_c = 3.69$, $\xi_0 = 2500$ Å, and $\rho l = 1100$ $\mu\Omega$ cm Å.

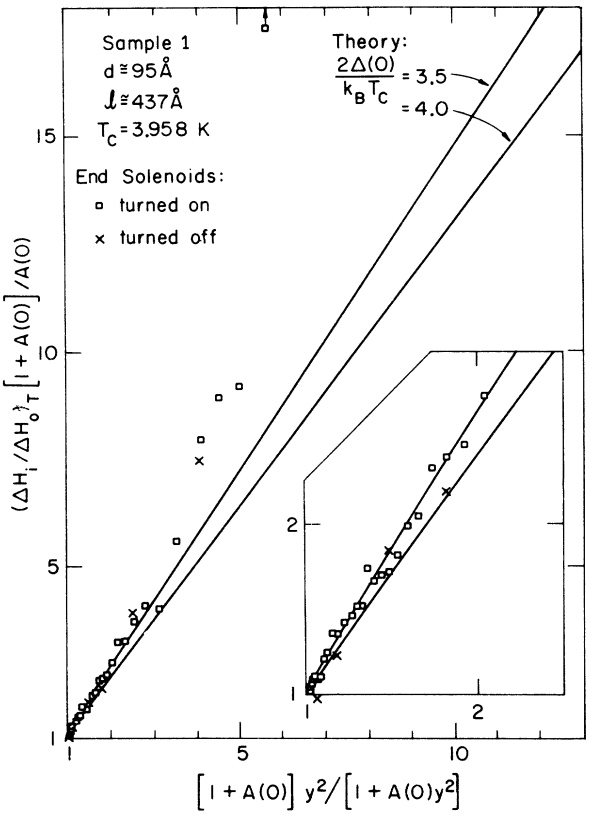

FIG. 4. Magnetic field attenuation ratio for sample 1.

E), it was also allowed to be a variable in Table II. The main uncertainties in our value for λ_L are a result of the uncertainty in our knowledge of ξ_0 and ρl. Our experimental error is comparatively negligible. For the reasonable values $\xi_0 = 2500$ Å and $\rho l = 1100$ $\mu\Omega$ cm Å, the values of $\lambda_L(0)$ for each of our four thin films were within the range 397 ± 22 Å, as shown in Table II.

Our value for $\lambda_L(0)$ is in approximate agreement with the value of 350 Å determined indirectly by Toxen from critical-field measurements on films at least 650 Å thick,[57] but is larger than the bulk indium values 250 Å, determined by Fossheim from ultrasonic attenuation measurements,[59] and 205 Å, determined by Dheer from rf surface-impedance measurements.[55] Our value for $\lambda_L(0)$ is much larger than that which would be calculated from typical values of the Ginzburg-Landau parameter[60]

$$\kappa(0) = 0.96\lambda_L(0)/\xi_0 + 0.73\lambda_L(0)/l \qquad (14)$$

for bulk indium. Feder and McLachlan[58] have obtained a determination of κ equal to 0.062 for pure indium from measurements of superheating and supercooling on essentially bulk specimens. For a coherence length of 2500 Å, the corresponding value of the London penetration depth at absolute zero would be approximately 160 Å, in agreement with the theoretical value from the free-electron model. However, if the theoretical London penetration depth for indium is renormalized,[58] a value of 380 Å is obtained, in agreement with our result.

Chang and Serin have determined κ and l from measurements of the transverse critical field for thin indium films.[61] Taking the ideal coherence length ξ_0 to be 2500 Å and using their data, we calculate $\lambda_L(0)$ to be 260 Å for their 5500-Å-thick film, and 350 Å for their 230-Å-thick film. These values are larger than Fossheim and Dheer's bulk indium results, and are smaller than the determination for our thinner films. This trend would appear to indicate that the London penetration depth increases with decreasing film thickness.

The apparent dependence on the London penetration depth on film thickness might be a result of the increasing importance of the surface for decreasing film thickness. This surface effect is also indicated by the increase in the superconducting transition temperature of small specimens, which is thought to be due in part to a change in the phonon spectrum,[62] and in part to a change in the electron mean free path.[63] These changes may affect the electronic structure of the material, and hence $\lambda_L(0)$. Of course, the film thickness may also have a direct effect on the electronic structure, including a reduction in the effects of crystal anisotropy.

C. Temperature Dependence of the Magnetic Field Attenuation Ratio

Values of the magnetic field attenuation ratio are plotted in Figs. 4–7 for temperatures from 1.3 K to a temperature which is within 100 or 200 mK of the transition temperature. Instead of using a scale linear in temperature as the abscissa, which would concentrate the variation of the attenuation ratio to one side of the plot, we have chosen to use a parameter which reflects the temperature dependence of the magnetic field penetration according to the two-fluid model.[1] According to this model, the temperature dependence of λ is given by

$$\lambda = \lambda(0)y\ , \qquad (15)$$

where

$$y = [1 - (T/T_c)^4]^{-1/2}\ . \qquad (16)$$

Combining this with Eqs. (3) and (7) we see that $\Delta H_i/\Delta H_0$ should vary as indicated by Eq. (6), but with

$$A(T) = A(0)y^2 \qquad (17)$$

according to the two-fluid model. Therefore,

$$(\Delta H_i/\Delta H_0)_{\text{two fluid}} = A(0)y^2/[1 + A(0)y^2]\ . \qquad (18)$$

To indicate the deviation of the data from the pre-

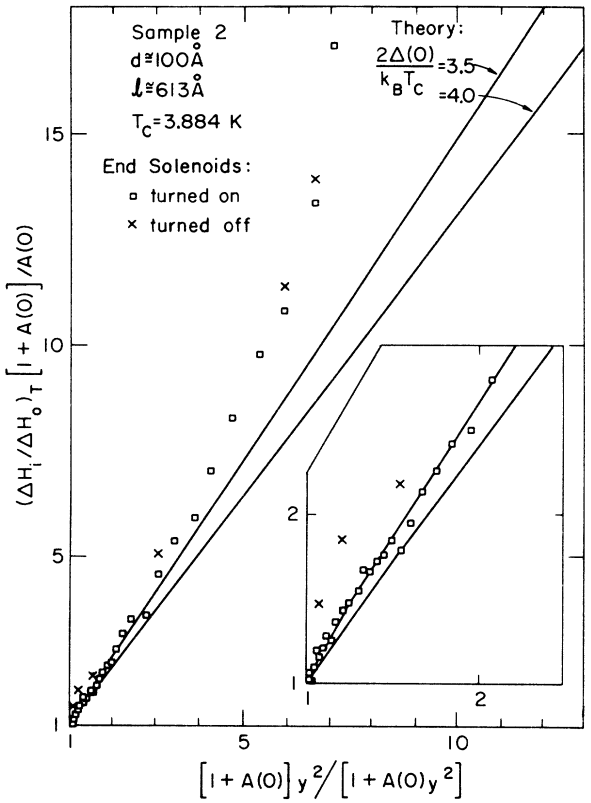

FIG. 5. Magnetic field attenuation ratio for sample 2.

diction of the two-fluid model, we would therefore plot $\Delta H_i/\Delta H_0$ against $A(0)y^2/[1+A(0)y^2]$. Because we have determined $A(0)$ by fitting the data to Eq. (6), both the measured and the theoretical values of the magnetic field attenuation ratio at absolute zero are given by $A(0)/[1+A(0)]$. To normalize the plots, both coordinates in Figs. 4–7 have therefore been divided by this constant, as indicated in the figures. According to the two-fluid model, the data would fall on a straight line with slope 1, passing through the lower left-hand corner of each plot. [The values of $A(0)$ for our four samples are listed in Table II.]

To compare our results with the BCS theory, we have indicated in the figures the temperature dependence predicted by Eqs. (6) and (7). In evaluating $K(0, T)$ from Eq. (5), we have used gap values $\Delta(T)$ which are scaled up from the theoretical values[20] by a constant multiplier. We have done this because the measured reduced gap width appears to be somewhat larger than indicated by weak-coupling (BCS) theory.[17] Experiments show that $\Delta(T)/\Delta(0)$ varies with temperature as indicated by the BCS theory, even for strong-coupling materials.[64]

Except for sample 4 and for temperatures within about 0.3 K of T_c ($y^2 > 3.5$), the data are much better fitted by the BCS temperature dependence (with reasonable values of the energy gap) than by the two-fluid model or by most other experimental results.[1,2] Disregarding sample 4, the reduced energy gap $2\Delta(0)/k_B T_c$ appears to be between 3.5 and 4.0, according to our data. However, we estimate that errors in $A(0)$ on the order of 10% or larger may have resulted from uncertainties in the measurements of the magnetometer stray sensitivity (see Sec. III B). Such errors would affect the vertical scales of Figs. 4–7, so that the reduced energy gap cannot be determined conclusively. The poor fit for sample 4 may be the result of a relatively large error in $A(0)$, because of the smallness of $A(0)$ for sample 4 ($\sim 3.5 \times 10^{-4}$). The indication that the magnetic field penetration near T_c is larger than theoretically predicted may be the result of film inhomogeneity; T_c may have been slightly different for different regions of a given film. Our films had transition widths on the order of 0.1 K, as shown in Table I. Therefore, it is evident that the films were not ideal. The data show a deviation from the theoretically expected temperature dependence which could be accounted for by assuming that the criti-

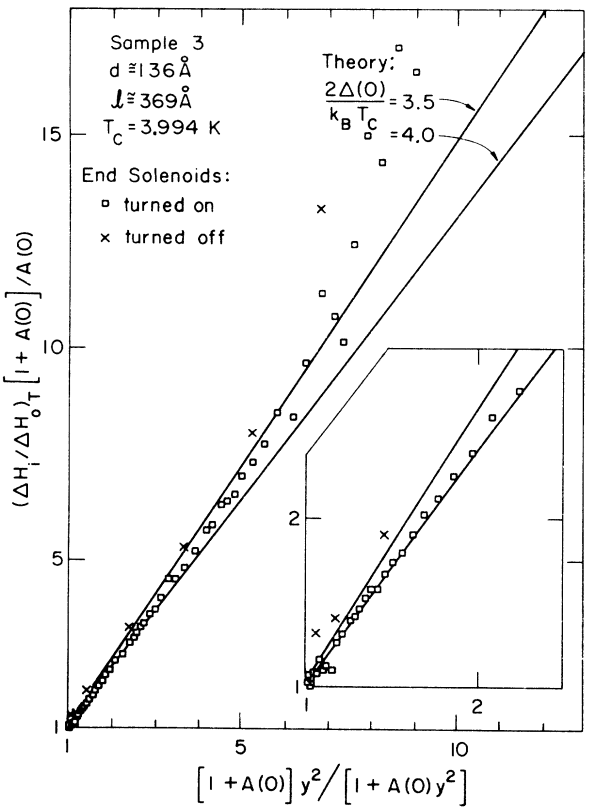

FIG. 6. Magnetic field attenuation ratio for sample 3.

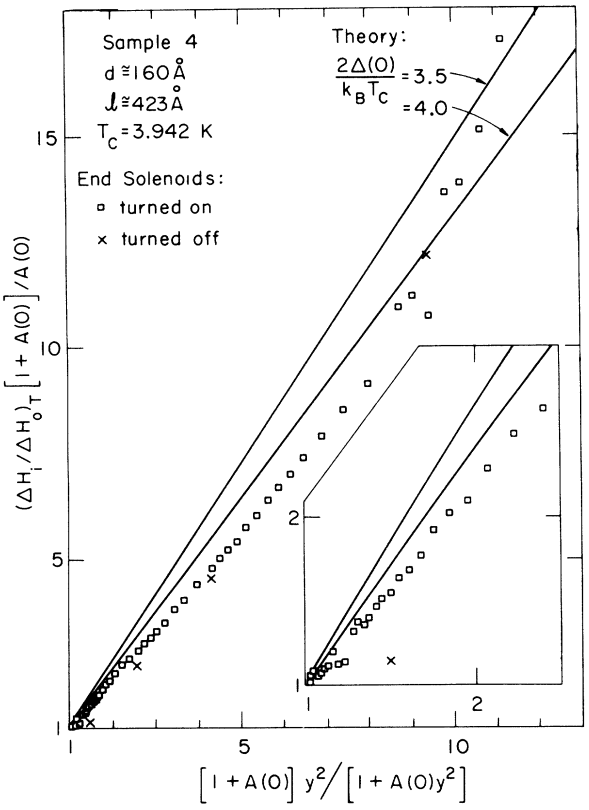

FIG. 7. Magnetic field attenuation ratio for sample 4.

cal temperature is effectively near the low-temperature tail of the resistive transition.[30]

We have determined the London penetration depth that would result from adjusting the values of $A(0)$ so that the data are better fitted by the theoretical prediction for a reduced energy gap of 3.69 [56] in the temperature range for which $y^2 \leq 1.8$. In doing this we sacrifice the absolute nature of the measurements, and ignore the possible effects of Fermi-liquid interactions.[65] [The value of $A(0)$ for sample 1 did not appear to need correction.] We obtained in this way the estimates of the London penetration depths shown in the right-hand column of Table II, for the reasonable values $\xi_0 = 2500$ Å and $\rho l = 1100$ $\mu\Omega$ cm Å. Those results are empirically fitted by the expression

$$\lambda_L(0) = 280 \text{ Å} + 11\,000 \text{ Å}^2/d \ . \qquad (19)$$

The extrapolation of this expression to infinite thickness yields a bulk value of 280 Å, in good agreement with Fossheim's measurement of 250 Å.[59] Of course, the approximately 95- to 160-Å range of d involved in the empirical fit is really too restricted to justify an extrapolation to bulk samples.

D. Reliability of Data

By deliberately subjecting the samples to abnormal experimental conditions, we determined that the experimental results were not particularly sensitive to the experimental conditions. The effects of not compensating at all for magnetic field fringing at the ends of the cylindrical film (end solenoids turned off) may be seen in Figs. 4–7 to be small. The lack of consistency in the sign of the effect in different samples is probably the result of errors in the determination of the magnetometer stray sensitivity (see Sec. III B), which was different when the end solenoids were turned off than when they were turned on. Likewise, the application of a static transverse magnetic field as large as 0.4 G (much larger than the few mG residual transverse field present when the horizontal ambient field was properly canceled) or tilting the main field coils as much as 3° out of alignment with the sample axis had only small effects (a few percent), which were comparable to the scatter in each set of data.

To test the uniformity of the indium films, we measured the magnetic field attenuation ratio at points other than at the center of symmetry by moving the magnetometer probe along the sample's axis. The attenuation ratio varied with position by 6% or less for a variation in position of 3 mm. This was not significant compared to the other uncertainties; a 6% variation in the attenuation ratio would lead to less than a 3% shift in our value for $\lambda_L(0)$.

Two other possible sources of error were considered. Pinholes, if present in the sample, would be expected to allow magnetic field leakage through the cylinder wall. However, no pinholes large enough to be seen with the unaided eye were found in our indium films. Perhaps the glow discharge cleaning of the substrate removed the contamination that would have resulted in pinholes. If a sample had them, the magnetic field leakage would have been generated by a perturbation in the film's persistent current density which would be equivalent in lowest order to a magnetic quadrupole moment; the field perturbation would then decrease very rapidly as a function of distance from the pinholes. Even if a sample had several pinholes large enough to be visible, say 0.2 mm in diameter, the perturbation in the magnetic field H_i at the location of the probe loop would have been insignificant. The 10% anisotropy of the penetration depth of indium[55] might be expected to affect the results if preferred crystal growth relative to the plane of the substrate occurred during the time the sample was annealed at room temperature. However, the relatively short mean free path would be expected to remove the effect of the anisotropy.[66]

It was possible to check the reliability of our data by comparing the measured and calculated values of the actual penetration depth $\lambda(0)$ [as opposed to $\lambda_L(0)$]. Because the films were thin compared to λ, the response of the electrons to the applied field is a local one, and Eqs. (1) and (3) should apply. Equating $A(0)$ to $2\lambda^2(0)/ad$, we obtain "measured" values of $\lambda(0)$. Values of $\lambda(0)$ may be independently calculated from the residual resistivity and the gap parameter of each film. As a consequence of the relation between penetration depth and conductivity[67] and the Ferrell-Glover-Tinkham sum rule, [68,69] the penetration depth in a thin film is given in Gaussian units by

$$\lambda^2 = c^2/8A'\sigma_n \,, \tag{20}$$

where σ_n is the normal state conductivity and $A'\sigma_n$ is the strength of the δ function in the real part of the complex conductivity of the superconductor at zero frequency. Harris[70] has calculated A' for indium from tunneling data of Dynes, [56] and obtained the value $4.44\,\Delta(0)/\hbar$. Using this value, and taking the reduced energy gap to be 3.69, [56] we calculated values of $\lambda(0)$. The measured and calculated values of $\lambda(0)$ are listed in Table II are in good agreement.

Another check on the consistency of our interpretation of the data can be made by calculating a theoretical value of $\lambda_L(0)$. We combine Eq. (2) with the equations

$$\rho l = mv/ne^2 \tag{21}$$

and[17]

$$\xi_0 = \hbar v/\pi\Delta(0) \tag{22}$$

(where v is the Fermi velocity) to find that

$$\lambda_L(0) = [\hbar c^2 \rho l/4\pi^2 \xi_0 \Delta(0)]^{1/2} \,. \tag{23}$$

We have calculated values for $\lambda_L(0)$ from Eq. (23), using the value[56] $\Delta(0) = 0.541$ meV. The ratio of the values for $\lambda_L(0)$ shown in Table II to those given by Eq. (23) are shown in Table III. We feel that the deviation of this ratio from unity is sufficiently small to support the validity of our theoretical understanding of the penetration depth in thin films.

E. Flux-Creep Rate

In our early, preliminary measurements, it quickly became clear that observed values of the maximum magnetic field difference $\Delta H(T)$ across the film were an order of magnitude smaller than values which would be expected if there were no motion of quantized fluxoids in the films. [71] Therefore, we became interested in also using our samples to investigate fluxoid motion and pining. In the theoretical work of Anderson, [11] and of Anderson and Kim, [12] flux lines or bundles of such lines are assumed to become pinned in potential wells in the superconductor. The flux lines are released by the combined effects of driving forces, such as magnetic forces generated by the applied field[72,73] and those associated with thermal activation. The Anderson theory predicted that the magnetic flux in a superconductor would relax toward the critical state[10] by an amount proportional to the logarithm of the elapsed time after the applied magnetic field had been changed sufficiently to cause flux flow. Such a logarithmic time dependence was first reported by Kim *et al.* for hollow superconducting cylinders, [74] and has been observed for solid superconducting cylinders by Beasley *et al.* [75] who used a superconducting magnetometer similar to ours. Beasley *et al.* observed that the logarithmic creep rate depended linearly on the critical current density, in agreement with the Anderson-Kim theory. They observed only a weak dependence on temperature, and assumed that other parameters, such as the activation energy and bundle-size parameter, may depend strongly enough on temperature to overwhelm the linear temperature dependence which is otherwise expected to result from thermal activation. The question of whether or not flux creep is thermally activated appears to remain controversial; Wade has reported evidence against thermal activation. [76]

We observed a logarithmic proportionality to elapsed time over a time span of a factor of 1000, from times starting about 0.2 sec after the increment in the applied magnetic field. We define the logarithmic-creep rate to be

$$R_c = \frac{dH_i}{d\log_{10} t} \,. \tag{24}$$

Data for sample 2 (typical of data for the other three samples) are plotted as a function of temperature in the upper-half of Fig. 8. The error bars are estimates of one standard deviation in the mean values of 4–10 measurements for each point. A

TABLE III. Ratios of the experimentally determined values as shown in Table II to the values given by Eq. (23).

Sample	ρl ($\mu\Omega$ cm Å)	Using $\lambda_L(0)$ found for ξ_0(Å) = 2000	2500	3000	3500	4000	Using $\lambda_L(0)$ found from temp. dependence [a]
1	700	1.09	1.09	1.10	1.10	1.10	
	1100	1.07	1.08	1.08	1.09	1.09	1.08
	1500	1.04	1.06	1.07	1.07	1.08	
2	700	1.06	1.06	1.07	1.07	1.07	
	1100	1.03	1.04	1.05	1.05	1.06	1.08
	1500	1.00	1.02	1.03	1.04	1.04	
3	700	1.03	1.04	1.04	1.04	1.05	
	1100	1.01	1.02	1.02	1.03	1.03	0.98
	1500	0.99	1.00	1.01	1.02	1.02	
4	700	1.16	1.16	1.17	1.17	1.18	
	1100	1.13	1.14	1.15	1.15	1.16	0.96
	1500	1.10	1.12	1.13	1.14	1.14	

[a] Calculated according to Ref. a of Table II.

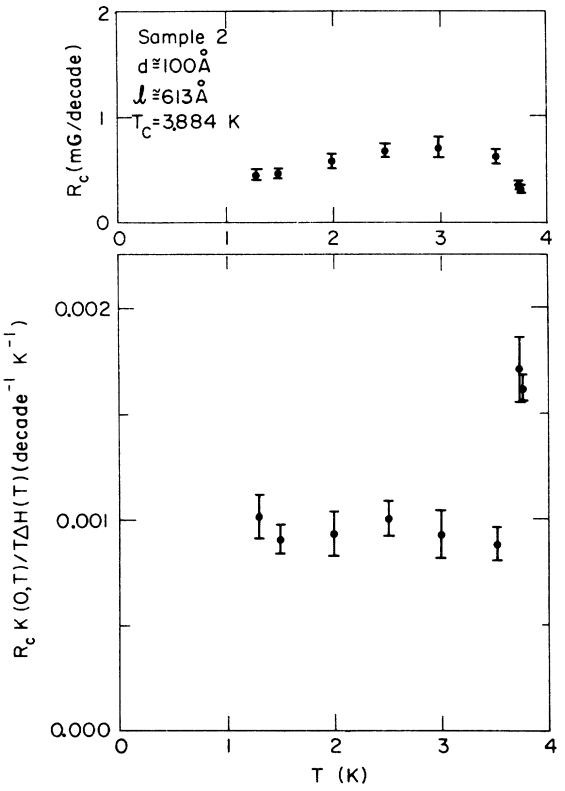

FIG. 8. Logarithmic flux-creep rate R_c, defined in Eq. (24) for sample 2. In the lower-half of the figure, R_c is normalized as explained in Sec. IV E to show the empirically observed dependence of R_c on temperature, critical-current density, and penetration depth.

weak but regular temperature dependence of R_c was apparent. The magnitude of R_c did not appear to depend appreciably on the film thickness.

According to the theory of Anderson and Kim, R_c should be proportional to the critical current density J_c, which in turn is proportional to the maximum magnetic-field difference across the film $\Delta H(T)$. (The critical current densities at $T \ll T_c$ for our films were calculated from the ΔH data to be on the order of 10^6 A/cm^2.) The flux creep was measured after a sweep of the applied field H_0 had been stopped along the linear "side" of a hysteresis loop. As shown in Fig. 9, the "sides" of hysteresis loops for sufficiently large amplitude sweeps of H_0 are lines of slope 1, displaced by ΔH to either side of the line $H_i = H_0$. Figure 9 also shows the smoothed ΔH data for sample 2; the temperature dependence is typical of all four samples. Near T_c the temperature dependence is similar to the theoretical dependence of the critical current[77]

$$J_c(T) = J_c(0)[1 - (T/T_c)^2]^{3/2} . \quad (25)$$

The temperature dependence was approximately linear in $T_c - T$ at lower temperatures.

The ratio of R_c to $T\Delta H(T)$ was roughly independent of temperature at lower temperatures, but increased sharply with temperature near T_c. The temperature dependence appeared to be similar to that of the magnetic field attenuation ratio, as if the logarithmic-creep rate also depended on $\lambda^2(T)$, which would be a kind of equivalent area occupied by the current circulating around each flux line. This temperature dependence was quantitatively tested in the following way. We expect that in the local-response limit of our films λ^2 is inversely proportional to the superconducting conductivity,[67] which in turn is proportional to $K(0, T)$ according to Eq. (4). Therefore, we divided $R_c/T\Delta H(T)$ by $K(0, T)^{-1}$. The result of this operation for sample 2 is shown in the lower-half of Fig. 8; the curve indicates a roughly temperature-independent function.

It may be recalled that Figs. 4–7 show that the magnetic-field penetration near T_c increased more rapidly with increasing temperature than theoretically predicted. This effect was most evident for the thinnest sample, sample 1, and was least evident for the thickest, sample 4. Remarkably, the temperature dependence of $R_c K(0, T)/T\Delta H(T)$ showed a similar trend.

V. SUMMARY

We have determined the London penetration depth λ_L

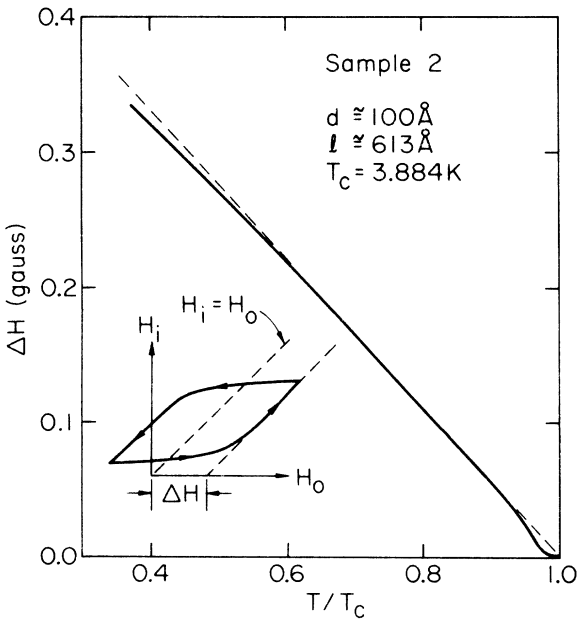

FIG. 9. Smoothed data showing the maximum magnetic field difference $H_0 - H_i$ for sample 2.

for indium films by a novel technique. Extrapolation to absolute zero indicates that $\lambda_L(0) = 397 \pm 22$ Å if one assumes that $\xi_0 = 2500$ Å and $\rho l = 1100$ $\mu\Omega$ cm Å. For other values of ξ_0 and ρl, values of $\lambda_L(0)$ are listed in Table II. There is some evidence that $\lambda_L(0)$ is somewhat larger for thin films than for bulk samples, indicating an altered electronic structure. The temperature dependence of the data is in moderately good agreement with the BCS theory (without Fermi-liquid corrections). Extrapolated to low temperature, the observed penetration depth $\lambda(0)$ is in good agreement with that which has been theoretically calculated from the gap parameter and renormalization function yielded by analyzing tunneling data on indium.

Magnetic flux creep has also been observed, with the expected logarithmic time dependence.

Now that we have developed and tested the techniques reported here, we are using them to investigate the electromagnetic properties of lead (a strong-coupling superconductor), of superconductors with paramagnetic impurities, and of superconductors which are influenced by the proximity effect.

ACKNOWLEDGMENTS

One of us (RAA) is grateful for fellowship support from the Allied Chemical Corp. and from the E. I. DuPont de Nemours Co. We are indebted to R. E. Harris for his calculation of the complex conductivity of superconducting indium, which was used in checking the reliability of our data and interpretation. J. M. Rowell and R. C. Dynes kindly supplied the tunneling data (Ref. 56) which were used by R. E. Harris in his calculation. We thank R. A. Banjavic for helping to acquire and reduce the data.

---

*Research supported in part by the Advanced Research Projects Agency, under Contract No. HC 15-67-C-0221 and in part by the National Science Foundation.

†Paper based in part on the Ph. D. thesis of Robert A. Anderson (University of Illinois, 1971) (unpublished).

‡Present address: Sandia Research Laboratories, Albuquerque, N. M. 87115.

[1]R. Meservey and B. B. Schwartz, in *Superconductivity*, edited by R. D. Parks (Marcel Dekker, New York, 1969), Vol. 1, p. 117.

[2]P. M. Tedrow, G. Faraci, and R. Meservey, Phys. Rev. B 4, 74 (1971).

[3]J. Clarke, Phil. Mag. 13, 115 (1966).

[4]J. Clarke and T. A. Fulton, J. Appl. Phys. 40, 4470 (1969).

[5]A. L. Schawlow, Phys. Rev. 109, 1856 (1958).

[6]E. Erlbach, R. L. Garwin, and M. P. Sarachik, IBM J. Res. Develop. 4, 107 (1960).

[7]M. P. Sarachik, R. L. Garwin, and E. Erlbach, Phys. Rev. Letters 4, 52 (1960).

[8]R. Jaggi and R. Sommerhalder, Helv. Phys. Acta 33, 1 (1960).

[9]K. E. Drangeid, R. Sommerhalder, H. Müller, and H. Seitz, IBM J. Res. Develop. 8, 13 (1964).

[10]C. P. Bean, Phys. Rev. Letters 8, 250 (1962).

[11]P. W. Anderson, Phys. Rev. Letters 9, 309 (1962).

[12]P. W. Anderson and Y. B. Kim, Rev. Mod. Phys. 36, 39 (1964).

[13]M. Tinkham, Phys. Rev. 129, 2413 (1963).

[14]J. R. Waldram, Advan. Phys. 13, 1 (1964).

[15]See A. B. Pippard, in *Advances in Electronics and Electron Physics*, edited by L. Marton (Academic, New York, 1954), Vol. 6, p. 1.

[16]R. Meservey, in *Proceedings of the Ninth International Conference on Low-Temperature Physics, Columbus, Ohio*, 1964, edited by J. G. Daunt *et al.* (Plenum, New York, 1965), Pt. A, p. 455.

[17]J. Bardeen, L. N. Cooper, and J. R. Schrieffer, Phys. Rev. 108, 1175 (1957).

[18]D. C. Mattis and J. Bardeen, Phys. Rev. 111, 412 (1958).

[19]A. B. Pippard, Proc. Roy. Soc. (London) A216, 547 (1953).

[20]B. Mühlschlegel, Z. Physik 155, 313 (1959).

[21]M. Peter, Phys. Rev. 109, 1857 (1958).

[22]Viton O rings are made to withstand moderate heating (Buckeye Rubber and Packing Co., Cleveland, Ohio).

[23]Apiezon N grease is a vacuum grease (Apiezon Products, Ltd., England).

[24]Model DTM-3 thickness monitor, Sloan Instruments Corp., Santa Barbara, Calif.

[25]L. Holland, *Vacuum Deposition of Thin Films* (Wiley, New York, 1958).

[26]S. Tolansky, *Multiple-Beam Interferometry of Surfaces and Films* (Oxford, U. P., London and New York, 1948).

[27]H. van Paassen, Rev. Sci. Instr. 32, 871 (1961).

[28]Inorganic silver micropaint SCP12 (Micro-Circuit Co., New Buffalo, Mich.).

[29]Resistance per square is defined to be the resistance which would be measured for a square piece of the film, with electrodes attached along the entire lengths of two opposite sides. Hence, the resistance per square is equal to the resistivity divided by the film thickness.

[30]Robert A. Anderson, Ph. D. thesis (University of Illinois, 1971) (unpublished).

[31]Type A-25 niobium 25% zirconium wire with copper plating and Formvar insulation (National Research Corp., Supercon Division, Natick, Mass.).

[32]C. Blake and C. E. Chase, Rev. Sci. Instr. 34, 984 (1963).

[33]A. C. Anderson, Rev. Sci. Instr. 39, 605 (1968).

[34]H. R. Hart, Jr., Ph. D. thesis (University of Illinois, 1960) (unpublished).

[35]D. M. Ginsberg and M. J. Melchner, Rev. Sci. Instr. 41, 122 (1970).

[36]Model 1072 signal averager (Fabritek, Inc., Madison, Wisc.).

[37]Model 3400 digitizer (Auto-Trol Corp., Arvada, Colo.).

[38]K. Fuchs, Proc. Cambridge Phil. Soc. 34, 100 (1938).

[39]G. K. White and S. B. Woods, Rev. Sci. Instr. 28, 638 (1957).

[40]C. A. Swenson, Phys. Rev. 100, 1607 (1955).

[41]R. W. Powell, M. J. Woodman, and R. P. Tye, Phil. Mag. 7, 1183 (1962).

[42]A. V. Bassewitz and G. V. Minnigerode, Z. Physik 181, 368 (1964).
[43]L. V. DelVecchio and P. Lindenfeld, Phys. Rev. B 1, 1097 (1970).
[44]K. R. Lyall and J. F. Cochran, Phys. Rev. 159, 517 (1967).
[45]E. Guyon, F. Meunier, and R. S. Thompson, Phys. Rev. 156, 452 (1967).
[46]F. J. Blatt, A. Burmester, and B. LaRoy, Phys. Rev. 155, 611 (1967).
[47]F. de la Cruz, M. E. de la Cruz, and J. M. Cotignola, Phys. Rev. 163, 575 (1967).
[48]R. D. Chaudhari and J. B. Brown, Phys. Rev. 139, A1482 (1965).
[49]R. S. Thompson and A. Baratoff, Phys. Rev. Letters 15, 971 (1965).
[50]P. Wyder, Phys. Kondens. Materie 3, 263 (1965).
[51]A. M. Toxen, M. J. Burns, and D. J. Quinn, Phys. Rev. 138, A1145 (1965).
[52]K. Forsvoll and I. Holwech, Phil. Mag. 10, 181 (1964).
[53]P. Cotti, Phys. Letters 4, 114 (1963).
[54]B. N. Aleksandrov, Zh. Eksperim. i Teor. Fiz. 43, 399 (1962) [Sov. Phys. JETP 16, 286 (1963)].
[55]P. N. Dheer, Proc. Roy. Soc. (London) A260, 333 (1961).
[56]R. C. Dynes (unpublished).
[57]A. M. Toxen, Phys. Rev. 127, 382 (1962).
[58]J. Feder and D. S. McLachlan, Phys. Rev. 177, 763 (1969).
[59]K. Fossheim, Phys. Rev. Letters 19, 81 (1967).
[60]B. Serin, in *Superconductivity*, edited by R. D. Parks (Marcel Dekker, New York, 1969), Vol. 2, p. 925.
[61]G. K. Chang and B. Serin, Phys. Rev. 145, 274 (1966).
[62]A. Rothwarf, Phys. Letters 30A, 55 (1969).
[63]G. Bergmann, Z. Physik 228, 25 (1969).
[64]See, for example, S. Bermon and D. M. Ginsberg, Phys. Rev. 135, A306 (1964).
[65]A. J. Leggett, Phys. Rev. 140, A1869 (1965).
[66]P. W. Anderson, J. Phys. Chem. Solids 11, 26 (1959).
[67]R. E. Glover and M. Tinkham, Phys. Rev. 108, 243 (1957).
[68]R. A. Ferrell and R. E. Glover, Phys. Rev. 109, 1398 (1958).
[69]M. Tinkham and R. A. Ferrell, Phys. Rev. Letters 2, 331 (1959).
[70]R. E. Harris (private communication); Phys. Rev. B 2, 228 (1970).
[71]D. H. Douglass, Jr., Phys. Rev. 124, 735 (1961).
[72]J. Friedel, P. G. de Gennes, and J. Matricon, Appl. Phys. Letters 2, 119 (1963).
[73]Y. B. Kim, C. F. Hempstead, and A. R. Strnad, Phys. Rev. Letters 9, 306 (1962).
[74]Y. B. Kim, C. F. Hempstead, and A. R. Strnad, Phys. Rev. 131, 2486 (1963).
[75]M. R. Beasley, R. Labusch, and W. W. Webb, Phys. Rev. 181, 682 (1969).
[76]J. M. A. Wade, Phil. Mag. 20, 1107 (1969).
[77]J. Bardeen, Rev. Mod. Phys. 34, 667 (1962).